Pure Appl. Chem., Vol. 74, No. 9, pp. 1519–1526, 2002.

Structural variations in nanocrystalline nickel films*

Pratibha L. Gai[1,2,‡], Rahul Mitra[3,4], and Julia R. Weertman[3]

[1]DuPont, Central Research, Experimental Station, Wilmington, DE 19880-0356, USA; [2]University of Delaware, Department of Materials Science and Engineering, Newark, DE 19716, USA; [3]Northwestern University, Department of Materials Science, Evanston, IL 60208, USA; [4]Defence Metallurgical Research Laboratory, Hyderabad, India

Abstract: Nanocrystalline nickel films of technological importance have been grown on various liquid nitrogen-cooled substrates by magnetron sputtering with and without a substrate bias. The atomic structural and chemical studies have unveiled variations in inter- and intragranular structures under the different process conditions. The origin and the development of the crystallization process with and without the substrate bias voltage have been inferred from the results.

INTRODUCTION

Advanced nanostructured materials such as nanocrystalline metals have generated widespread interest internationally because they exhibit exceptionally high strengths [1,2]. The high strengths in the nanocrystalline metals are primarily the result of restricted dislocation activity in the tiny grains. Synthesis methods to produce nanocrystalline metals play a key role in their structure–property relationships and are, therefore, important. Methods that produce nanocrystalline powder (e.g., inert gas condensation and ball milling) and thus require compaction, lead to material that is subject to porosity, poorly bonded grains, impurities, and a broad dispersion in grain sizes [3,4]. In the present paper, we describe nanocrystalline Ni films produced by magnetron sputtering Ni atoms directly onto substrates. Nanocrystalline Ni is of technological interest with applications as protective layers [5] or contact layers in microelectronic circuitry [6]. The grain size and morphology of the films greatly affect the hardness properties on protective layers and conductivity in electrical devices. The mechanical properties of the nanomaterial films depend on the grain structure and size distribution and internal residual stress. A better fundamental understanding of nanostructure–property relationships in nanocrystalline films is, therefore, required to optimize their properties.

EXPERIMENTAL PROCEDURES

Nanocrystalline Ni films on various substrates have been synthesized by magnetron sputtering in order to explore the effect of different processing parameters on the grain size, surface porosity, and internal residual stresses. A dc magnetron source Mak2 (US Inc., San Jose, CA) was used which is designed to sputter magnetic materials and has been described elsewhere [2]. Briefly, the Ni cathode used in the studies was 99.99 % pure and was 50.8 mm in diameter and 3.175 mm in thickness. The base pressure

Pure Appl. Chem.* **74, 1489–1783 (2002). An issue of reviews and research papers based on lectures presented at the 2nd IUPAC Workshop on Advanced Materials (WAM II), Bangalore, India, 13–16 February 2002, on the theme of nanostructured advanced materials.
‡Corresponding author

used was between 10^{-7} and 10^{-6} torr. The cathode power was 200 W. The high-purity argon used was maintained at 6 mtorr pressure during deposition. A pulsed dc negative bias between 0 and 150 V was applied during the deposition using an ENI (Fremont, CA) power supply system. The pulse frequency and width were 250 kHz and 1296 ns, respectively. Application of a pulse supply to bias helps prevent charge build-up on the substrate.

Some samples were grown on holey carbon-filmed copper grid substrates held close to liquid nitrogen (LN) temperature using a substrate bias of –150 V (designated as sample I). In the present study, film thicknesses were generally ~0.1 μm (referred to as thin samples), but some were of higher thickness (~1.5 μm). Application of bias enhances the sputtering of the film by argon ions and leads to densification, which will be discussed in the following sections. Another set of samples was grown on NaCl substrates (with an adjacent Si substrate for thickness calibration) without the application of substrate bias (0 V bias), also at LN temperature (referred to as sample II). Nanocrystalline Ni films on NaCl substrates were floated off in water, and the films were supported on Cu grids for plan view imaging. The thin samples were electron-transparent. Thicker samples were thinned by argon ion beam milling at LN temperature. Samples grown on room temperature (RT) substrates have been described previously [2]. In the case of deposition with a negative bias, the grains in the RT films are larger than those of their counterparts grown at LN temperature. The increased grain size was attributed to greater atomic mobility at the warmer temperature. The present paper describes a detailed investigation of structural variations in samples processed at LN temperature with and without negative substrate bias.

We have obtained nanostructural data at atomic resolution and nanochemical data simultaneously using advanced high-resolution (scanning) transmission electron microscopes (TEMs), namely, novel FEI FE(S)TEM Tecnai [7], CM20 HRTEM, and novel Philips CM30 Environmental-TEM (ETEM) [8–10] with electron-accelerating voltage of 200 keV. Powerful FE STEM/TEM, the so-called 2-2-2 200 keV field emission Tecnai STEM/TEM combines atomic resolution imaging with atomic level chemical and crystallographic analyses with 2 Å (0.2 nm) resolution in each of the TEM, STEM, and chemical analyses modes (hence, 2-2-2), providing new opportunities in the nanomaterial sciences. The HR(S)TEMs were fitted with X-ray spectrometers. The detection of electron-stimulated X-ray emission in the electron microscope (energy-dispersive X-ray spectroscopy or EDX) permits simultaneous determination of chemical compositions of the nanomaterials to the subnanometer level. For nanochemical data, nanoprobe analyses were recorded using EDX in the electron microscopes. Additional analyses were also carried out in the ETEM after cleaning the samples in the ETEM to remove any contamination. The ETEM is fitted with a reaction (environmental) cell and a heating sample stage. Grain size distributions and the mean grain size were obtained by atomic-resolution HRTEM and dark-field TEM imaging of about 1000 grains. High-resolution low-voltage FESEM (LVSEM) was used for studies of film surface texture and roughness.

RESULTS AND DISCUSSION

The nanostructural and chemical data are quite informative. Previous studies have shown that samples processed at LN temperature both with and without a substrate bias have a <111> fiber texture, but this texture is weaker in the former case [2]. The <111> direction is the preferred orientation of the normal to the surface due to energy considerations, but the texture is weakened with grain growth, and grains with orientations other than <111> are also present. Our atomic structural studies of both samples I and II show that they contain nanocrystals with (111), as well as some with (100) and (110) surface planes. In sample I, HRTEM and dark-field TEM show grain sizes between a few nanometers (3 to 4 nm) to ~50 nm with the average (mean) grain size of 15 ± 2 nm. Grain structures in low- and high-resolution images of nanocrystalline sample I are shown in Figs. 1a and 1b, respectively. Figure 1c shows the selected area electron-diffraction pattern recorded from an area consisting of several grains, indicating the presence of (111), (200) planes. Additionally, we have carried out complex electron nanodiffraction

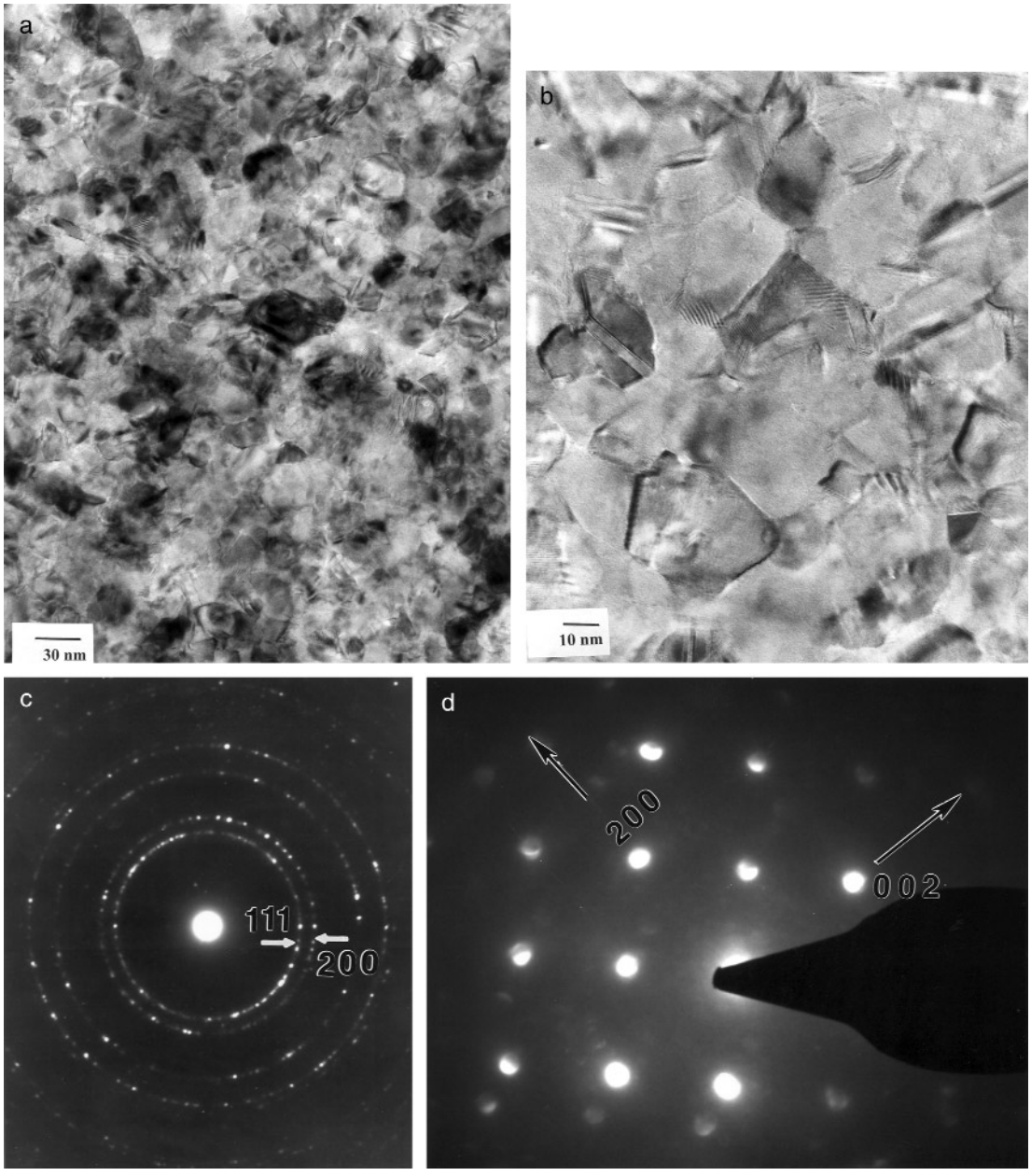

Fig. 1 Grain structures of nanocrystalline nickel films processed by magnetron sputtering at liquid nitrogen (LN) temperature with substrate bias (samples I). (a) low-magnification image; (b) high magnification; electron diffraction from an area of several nanograins showing the presence of, e.g., (111), (200) planes; (d) nanodiffraction from a single nano-Ni grain of ~2 nm in size in (010) crystal projection, recorded using electron probe size of 1 nm. 200 and 002 directions are shown. They are no longer normal to one another but deviate very slightly (~ by about 1º) from the bulk fcc structure. Careful studies of many nanodiffractions from very small grains (~1–2 nm), are consistent with the small deviation.

studies from single nanocrystalline Ni grains using electron probe size of a nanometer in the Tecnai FE(S)TEM. Figure 1d illustrates nanodiffraction from an individual Ni grain of only a couple of nm in size. Careful measurements of several nanodiffraction patterns from nanosized (1–2 nm) grains indicate that they deviate very slightly (by ~1°) from the bulk fcc structure, because the axes are no longer at 90° with respect to one another. Such minute structural deviations in nanoscale materials relative to their bulk structure, have also been observed in other nanomaterials, such as Bi nanoscale wire materials, and can give rise to interesting structural and electronic properties [11].

Defects in the grains are primarily twins, with a few interfacial defects as shown in the atomic structure images in Figs. 2a and 2b. Twin formation is favored as twin boundaries have a lower energy than high-angle grain boundaries. The high internal strains present in the films indicate that these defects could form as the films grow from the original nuclei and the growing nuclei meet at boundaries. In the atomic images, nanoporosity with pores of 1–2 nm is observed especially along grain boundaries. The lattice spacings and nanoprobe analyses using EDX spectroscopy are consistent with Ni, with no impurity segregation at the grain boundaries. We have not observed any amorphous intergranular regions (Fig. 2). There are Moiré fringes owing to overlapping grains (arrowed at m) and a few interfacial dislocations. The surface texture of the sample I film is shown in the LVSEM image shown in Fig. 3, recorded at 3 keV.

In sample II (zero substrate bias), nanoparticles have sizes in the range of a few nm to a few tens of nm and have increased porosity compared to sample I. The average (mean) grain size was estimated to be 12 ± 2 nm. Significantly, amorphous regions up to a few nanometers in extent are found in the interfacial regions between the nanocrystals (arrowed in Fig. 4a). The nature of the amorphous regions was confirmed by atomic resolution imaging and extensive sample tilting to different crystallographic orientations. The sample tilting showed no crystallinity in these regions. Electron diffraction from the nanocrystalline grains of sample II (shown in Fig. 4b) shows a stronger <111> texture than in sample I.

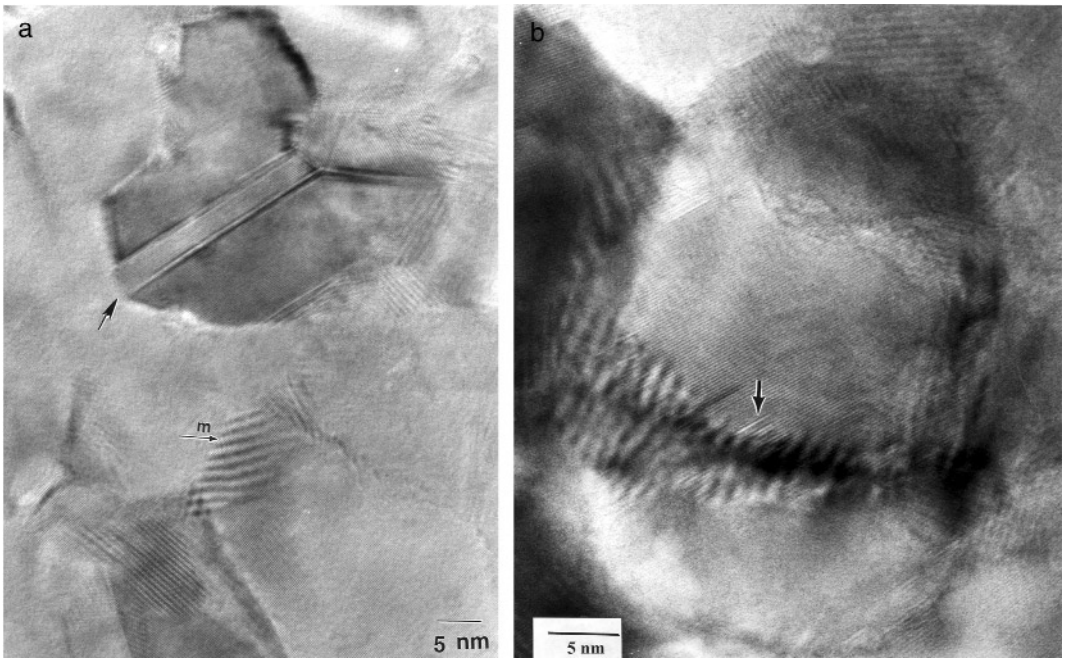

Fig. 2 (a) Twins (arrowed) and Moire fringes (m) in nanocrystalline Ni and (b) interfacial defects in nanocrystalline Ni (sample I).

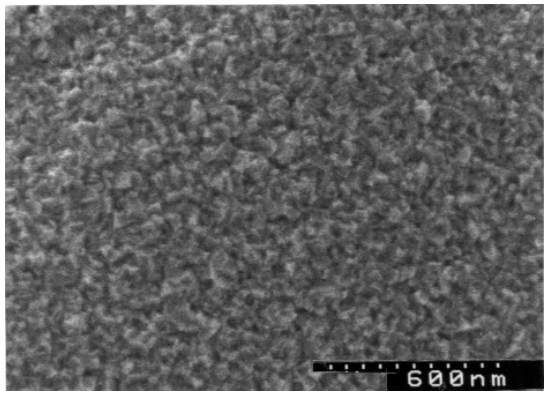

Fig. 3 Surface texture of nanocrystalline sample I recorded with LVSEM at 3 keV.

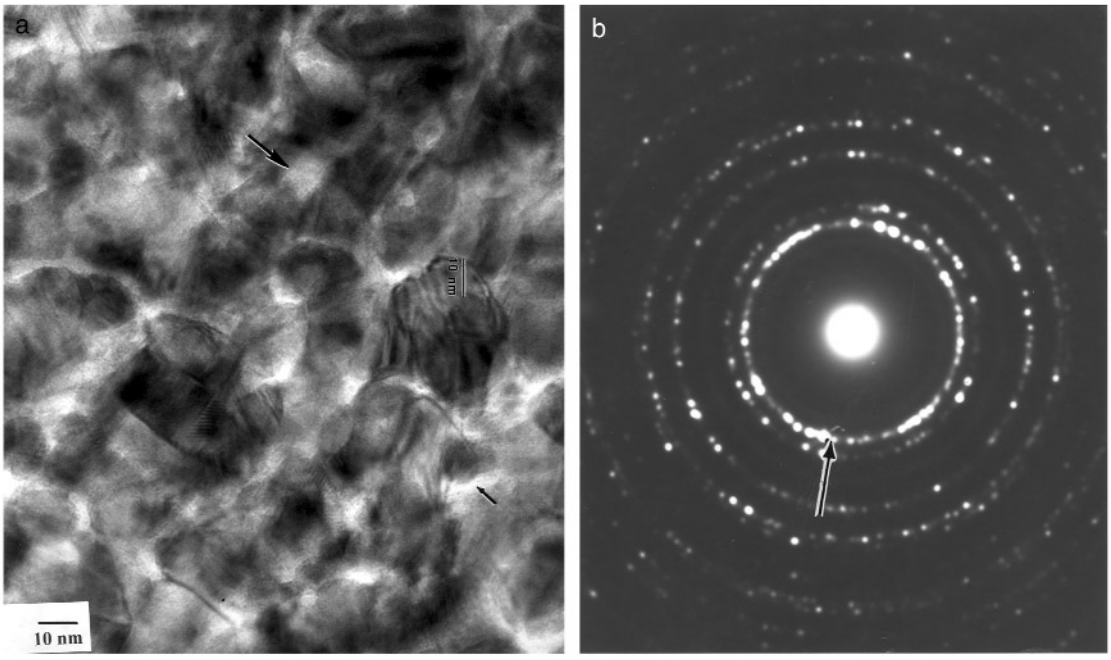

Fig. 4 (a) Amorphous intergranular regions in nanocrystalline Ni processed without substrate bias (samples II); (b) electron diffraction from sample II indicating a stronger <111> texture (indicated by an arrow).

High-precision FE-STEM nanoprobe analyses using STEM dark-field imaging in the Tecnai, illustrated in Fig. 5, have shown that intergranular regions shown in Fig. 4a are primarily amorphous Ni-rich regions. This direct evidence indicates that the crystallization is not complete in sample II. Some Ni nanoparticles (clusters) are also observed in amorphous regions near the edge of the films (Fig. 6). In general, our studies of sample II have shown that the Ni grains tend to be single crystals and have fewer intra- and intergranular defects compared to sample I. The origin and the development of the crystallization process with and without the substrate bias voltage have been inferred from the results and are discussed below.

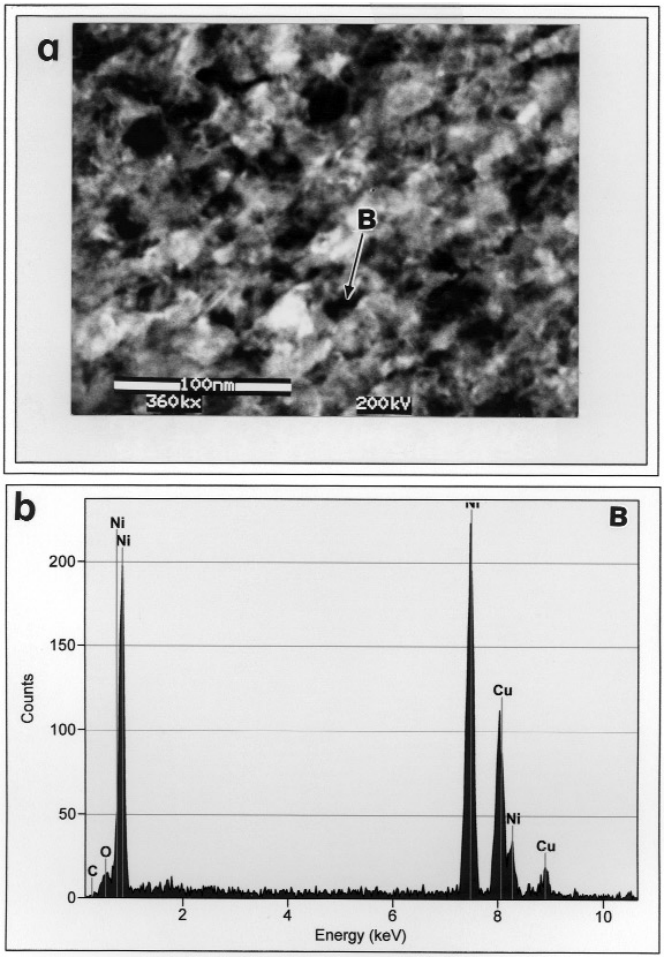

Fig. 5 (a) STEM dark-field (DF) image of nanometer-scale amorphous regions shown in Fig 4a. In the DF image, the amorphous regions (e.g., B) appear dark; (b) nanoprobe chemical composition analysis of the amorphous region B using EDX. The data show that the amorphous regions are Ni-rich.

GRAIN GROWTH OF NANOSTRUCTURED Ni FILMS

A substrate bias voltage leads to resputtering of adsorbed Ni atoms by argon atoms, thus enhancing their mobility through momentum transfer. This leads to a more uniform growth, equiaxed grains[2], improvement in density leading to the densification of the film, and the growth of the initial island nuclei until they impinge on one another. Thus, in sample I with the substrate bias, the growth of the nuclei and the densification of the film were achieved. Subsequent impingement of the crystalline islands leads to the formation of defects, including twins, and the overlapping grains lead to Moiré fringes. Furthermore, owing to an increase in the surface diffusion rates on resputtering of the film on the application of substrate bias, the mean grain size also tends to increase. The observations of (111) crystal planes and the presence of (110) and (100) suggest increased adatom mobility causing recrystallization.

In sample II, with no substrate bias and consequent absence of increased mobility from resputtering, the lack of significant thermal energy at LN temperature hinders the diffusion or redistribution of adsorbed Ni atoms needed to grow the crystalline nuclei. As a consequence, the interfacial regions

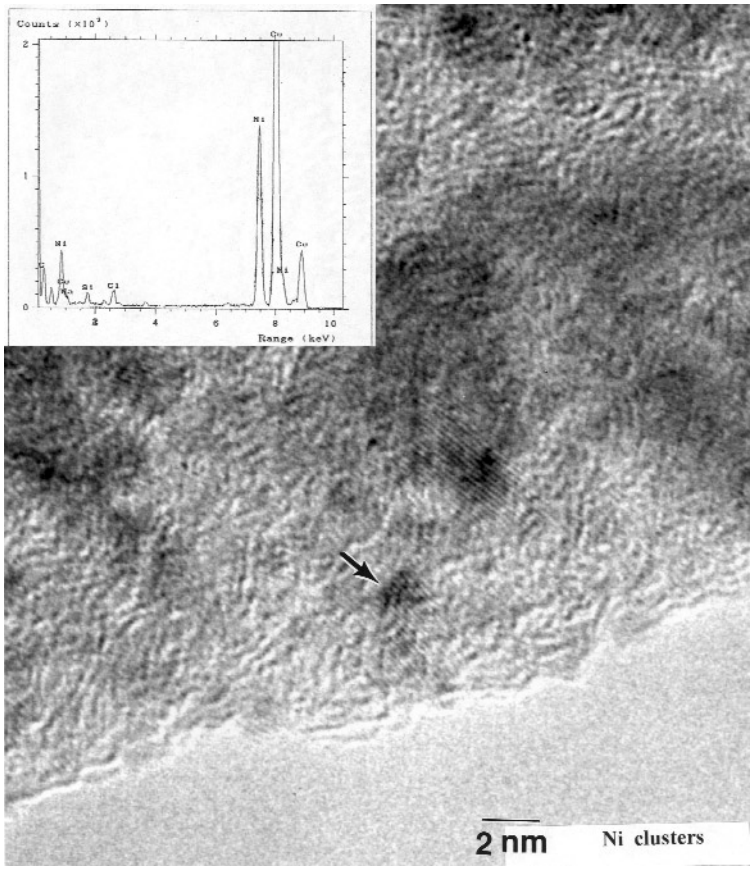

Fig. 6 Ni clusters (e.g., arrowed) in amorphous regions near the edge of the film, with chemical composition analysis of the clusters inset. The sample is on Cu microgrid. Cl and Si are due to the NaCl and Si substrates used in the experiments.

between grains are amorphous Ni-rich regions. The presence of amorphous interfacial regions does not seem to promote the formation of stacking defects. The lack of resputtering leads to columnar grain growth[2] in samples II.

The presence of amorphous nickel-rich regions may possibly be due to small amounts of impurities, especially gaseous impurities, which can inhibit crystallization and make Ni amorphous even at the fast cooling rates of 10^{12} K/s used in our experiments. Several studies of amorphous metals (metallic glasses) have been reported in the literature [12,13]. Davis et al. [12] have found that amorphous Ni is stabilized by small amounts (~0.7 wt %) of impurities with the critical cooling rate of 10^{10} K/s, and there are reports [14] that gaseous impurities as low as 1–2 at % can stabilize amorphous metal phases. High-precision X-ray spectroscopy data in our experiments suggest that very small amounts of N (at 0.392 keV) and O (at 0.52 keV) may be the gaseous impurities contributing to the stabilization of the amorphous nickel-rich phase.

Hardness values measured by nanoindentation on films ~1.5–2.5 μm thick sputtered on LN-cooled substrates with and without negative bias were generally found to be about 6 GPa, compared to hardness values in RT-sputtered counterparts of 4.5–6 GPa and 0.2–0.45 GPa for annealed coarse grain Ni [2]. The somewhat larger grain sizes at RT and the stronger <111> texture in the LN-cooled films may contribute to the higher hardness values in the latter class of films. Evidently, the presence

of amorphous intergranular regions or the columnar structures do not greatly degrade the hardness, at least as measured on the film surface.

ACKNOWLEDGMENTS

We thank L. G. Hanna, D. L. Smith, and F. G. Gooding for technical assistance.

REFERENCES

1. P. G. Sanders, J. A. Eastman, J. R. Weertman. *Acta Mat*. **45**, 4019–4029 (1997).
2. R. Mitra, R. A. Hoffman, A. Madan, J. R. Weertman. *J. Mater. Res*. **16**, 1010–1027 (2001).
3. R. Mitra, T. Ungar, T. Morita, P. G. Sanders, J. R. Weertman. In *Advanced Materials for the 21st Century*, Y.-W. Chung, D. C. Dunand, P. K. Liaw, G. B. Olson (Eds.), p. 553, TMS, Warrendale, PA (1999).
4. S. R. Agnew, B. R. Elliott, C. J. Youngdahl, K. J. Hemker, J. R. Weertman. *Mater. Sci. Eng*. *A* **285**, 391–399 (2000).
5. R. F. Bunshah. *Vacuum* **20**, 353–359 (1977).
6. K. N. Tu. *Treatise on Materials Science and Technology,* K. N. Tu and R. Rosenberg (Eds.), **24**, p. 157, Academic Press, NY (1995).
7. E. D. Boyes, J. Ringnalda, M. A. J. van der Stam, T. F. Flievoet, E. van Cappellen. *Microsc. Microanal.* **7**, 232–233 (2001).
8. P. L. Gai and K. Kourtakis. *Science* **267**, 661–663 (1995).
9. P. L. Gai. *Adv. Mater*. **10**, 1259–1263 (1998).
10. P. L. Gai, B. C. Smith, G. Owen. *Nature* **34**, 430–432 (1990).
11. S. B. Cronin, Y. M. Lin, O. Rabin, M. R. Black, G. Dresselhaus, M. S. Dresselhaus, P. L. Gai. *Microsc. Microanal.* **8**, 58–63 (2002).
12. H. A. Davis. *Metallic Glasses*, F. Luborsky (Ed.), Chap. 2, p. 8, Butterworths, London (1983).
13. H. A. Davis, J. Aucote, J. B. Hull. *Nature* **246**, 13–15, (1973).
14. P. H. Leung and J. B. Wright. *Phil. Mag*. 995–999 (1974).